N74-10279

Paper No. 56

METHOD AND RESULTS OF INFRARED TESTING OF THE HELIOS SOLAR PROBE

J. Guelpen and W. Lorenz,
ERNO Raumfahrttechnik GmbH, Bremen, Germany

ABSTRACT

The infrared test technique developed to test the HELIOS solar probe at intensities equivalent to up to 16 Solar-Constants is described. The principle of this technique and the design of a test facility derived from it are discussed. The particular application of this technique to the measurement of heat input into a solar irradiated aperture is presented. Test results are compared to solar simulation test results.

INTRODUCTION

The HELIOS solar probe is a spin stabilized spacecraft, which consists basically of a centerbody containing all the equipment and most experiments, a heat shield which protects the centerbody from the environment, and two conical solar arrays (see Fig. 1).

This spacecraft will approach the sun to 0.25 Astronomic Units (1 AU = distance earth - sun) and will pass through solar irradiation intensities up to 22,4 kW/m^2 or 16 Solar Constants (S.C.) which have never been encountered by a spacecraft before. It is obvious that the thermal design of this spacecraft should be verified by the most realistic space simulation tests possible.

The simulation of solar radiation by Xenon arc lamps has some slight inaccuracies as there are several deviations from solar radiation characteristics, e.g.

collimation of rays,
local intensity distribution,
spectral intensity distribution,
transient variations in local or
spectral distribution.

Nevertheless, the Xenon arc lamp has become the standard source for solar simulation and has proven to be highly accurate in most cases.

Unfortunately, there is no solar simulator available, which can provide 16 solar constants on a spacecraft of this size.

Therefore, there was no alternative but to simulate the solar heat input by infrared radiation.

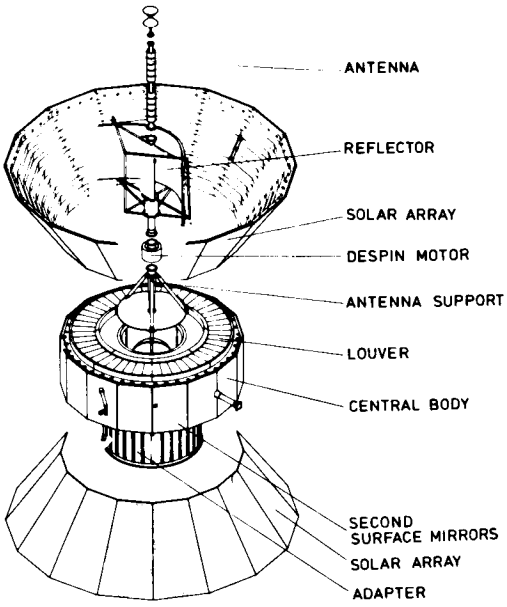

Fig. 1 HELIOS spacecraft

HELIOS INFRARED TEST TECHNIQUE

A heat balance of the HELIOS spacecraft shows that a very high amount of energy - 100 kW - is radiated onto the spacecraft (Fig. 2). Due to the particular design most of this energy is, however, directly reflected and emitted from the irradiated surfaces.

Only about 15 kW are conducted through the structure of the spacecraft - mainly through the solar panels - and emitted from other surfaces. From these figures it is readily apparent that an infrared test technique should try to simulate only the net heat flux through the spacecraft in order to reduce problems of power supply and energy transport in the space simulation chamber.

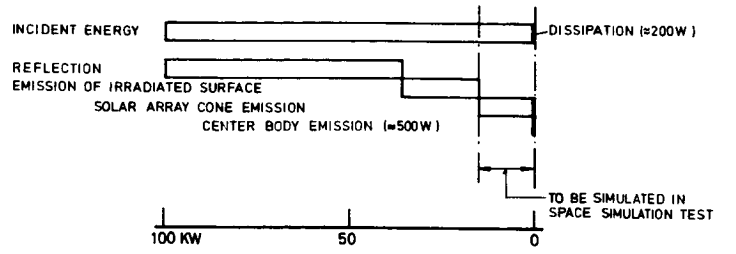

Fig. 2 HELIOS heat balance

Principle

Each thermal test technique should try to base its validity on as few assumptions and uncertainties as possible and, if uncertainties are unavoidable, their magnitude should be easily assessable and limited.

Therefore, the HELIOS infrared test technique is coupled as close as possible by means of tests and measurements to the Xenon arc lamp solar simulation. Use of complicated mathematical computer models and other sophisticated analytical means to establish the validity of the HELIOS infrared test technique are avoided. The reason for this is obvious: The validity of thermal test results should be completely independent of mathematical computer models of the spacecraft as the primary purpose of spacecraft thermal testing is to establish valid mathematical computer models by improving these due to test results.

The HELIOS thermal test technique is characterized by 3 steps which are described in the following.

Step 1: Determination of absorbed solar radiation incident to outer spacecraft surfaces.
The absorbed solar radiation is defined by

$$Q_{abs} = \alpha_s \cdot I_s \cdot e_s \cdot A \ , \qquad (1)$$

where

α_s is the solar absorptance of the surface for the particular solar light incident angle,

I_s is the solar intensity,

e_s is the cosine of the incident angle φ in the range $0 \leq \varphi \leq \frac{\pi}{2}$ ($e_s = 0$ for $\varphi \geq \frac{\pi}{2}$, of course) and

A is the area of the absorbing surface.

A sample of the surface, for which the absorbed solar radiation shall be determined, is equipped with a thin heater skin just below the surface coating, as it is shown in an example in figure 3. The heater skin shall have a low thermal resistance and the thermal contact resistance between heater skin and substrate on the one side and heater skin and surface coating on the other side shall be kept low too by use of adequate adhesive material, because electrical heating in the heater skin instead of simulated solar irradiation shall not essentially disturb the formation of lateral and longitudinal thermal gradients in the sample. The heater skin is designed to generate the heat quite uniformly over its total area.

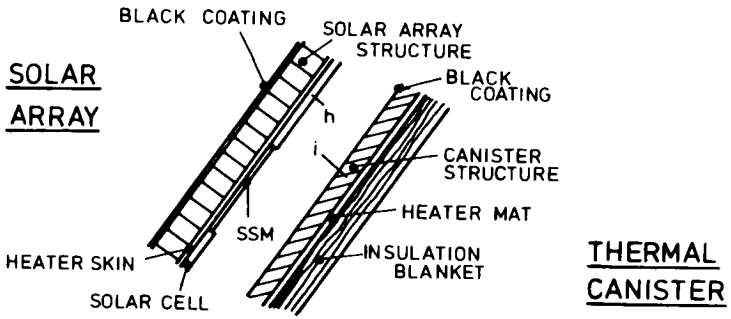

Fig. 3 Solar array infrared test set-up

Under simulated space conditions the sample is irradiated by simulated solar light with an intensity I_s and experiences equilibrium temperatures T_{h1}, T_{h2} ..... at different locations 1, 2 ..... a.s.o. Then the simulated solar light beam is switched off and the heater skin is heated by an electrical power Q_h which is regulated such that the sample experiences the same temperatures T_{h1}, T_{h2} ..... at the same locations as before. The absorbed heat Q_{abs} is determined by the electrical power Q_h.

$$Q_{abs} = Q_h \qquad (2)$$

The solar radiation, of course, is only uniformly absorbed by the sample area, if the absorptance α_s and the cosine factor e_s is uniform for the entire sample area.

However, under certain circumstances as are valid for the HELIOS solar arrays, for instance, the method of determining the absorbed heat as described above holds for surfaces with non-uniform α_s and e_s too. This will be discussed later.

Step 2: Calibration of infrared heater.
Simulated solar heating or electrical heating now is replaced by infrared heating. The infrared heater may be designed as shown in figure 3. However, the essential requirements are that the infrared heater emits the heat without local intensity variations and that the thermal conductance within the infrared heater along the surface is sufficiently low. The reason for the last requirement is discussed later.

The infrared heater is electrically heated with a heater power Q_i such that the irradiated sample exhibits the same temperatures T_{h1}, T_{h2} ..... at the same locations as in step 1. The net heat transfer Q_{net} between infrared heater and sample is equal to the difference between absorbed and emitted heat and is described by the equation

$$Q_{net} = \alpha_s \cdot I_s \cdot e_s \cdot A - \varepsilon_h \cdot A \, \sigma T_h^4 \qquad (3)$$

where

ε_h is the emittance of the sample surfaces and
σ is the Stefan-Boltzmann constant.

When the heat loss of the infrared heater through gaps between heater and sample is standardized by defining a fixed distance between both surfaces and/or avoiding heat losses from both surfaces by covering the circumferential gaps with highly reflective foil, the calibration of the infrared heater in form of a functional dependency

$$I_s = f(Q_i) \qquad (4)$$

can be established.

In case that there is suspicion that the thermal background environment of the infrared heater or the conductance of the infrared heater superinsulation may vary from test case to test case, it might even be better to establish a functional dependency

$$I_s = f(T_i^4) \qquad (5)$$

as a calibration curve.

522-137 O - 73 - 46

Step 3: Performance of thermal test.
The performance of the thermal test now can take place. The original irradiated surface, of course, is not equipped with a heater skin, but otherwise identical to the sample. The simulated solar intensity is controlled by using the calibration curves, eq. (4) or eq. (5).

Extension of Infrared Test Technique Applicability

For constantly rotating surfaces neither obviously e_s nor usually α_s is constant. The absorptance α_s usually is dependent on the incident angle. However, for rotating surfaces irradiated by solar light the described infrared heating technique can be applied too, if the angular velocity and/or the thermal capacity of the surface are high enough such that transient temperature variations during one revolution are negligible.

Furthermore, the method is applicable for surfaces with a coating pattern containing elements of different absorptances α_s provided that the surface substrate has a sufficiently high thermal conductance which allows only negligibly small temperature differences between the surface elements of different absorptance, or provided that not microscopical but only macroscopical temperature distribution is of interest.

An example for a rotating surface with a coating pattern of non-uniform absorptance is the HELIOS solar array. This array is a rotating conical surface with a pattern of solar cells, second surface mirrors (= optical solar reflectors) and gaps between cells and mirrors with different absorptances.

A further extension of the infrared test technique is possible for irradiated sensor apertures, which really cannot be called "surfaces" anymore, as they usually mainly consist of funnels. Here another parameter - the temperature level of the spacecraft interior - is influencing the net heat input to the "surface" and, therefore, complicates the infrared test technique. The availability of an applicable test technique in this case, however, is very important for HELIOS, as the heat absorbed by sensor apertures is of essential magnitude for solar probes.

Theoretical Basis of Sensor Aperture Infrared Heaters

In order to determine the heat input to apertures a special aperture test body for each of the sensor apertures has been built. An aperture test body consists of the aperture part (e.g. funnel) of the sensor, a heat shield part surrounding the sensor, a black heater plate, which exclusively has radiative heat exchange with the aperture part, and a surrounding superinsulation, in which only the sensor

aperture and a radiator area of the heater plate remains uncovered. The heater plate is black, as it represents the interior of the solar probe; it is used to sense the net heat input via sensor aperture into the probe interior. An example of an aperture test body is shown in figure 4 and the principle of an aperture test body with aperture infrared heater is shown in figure 5.

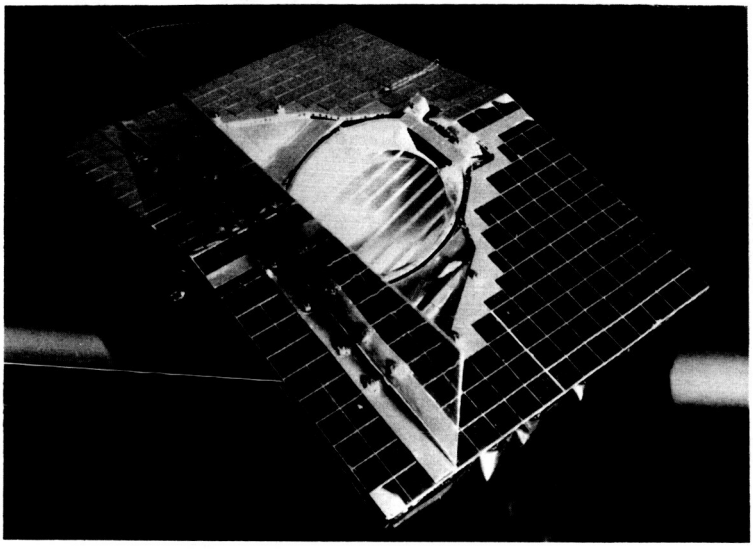

Fig. 4 Aperture test model

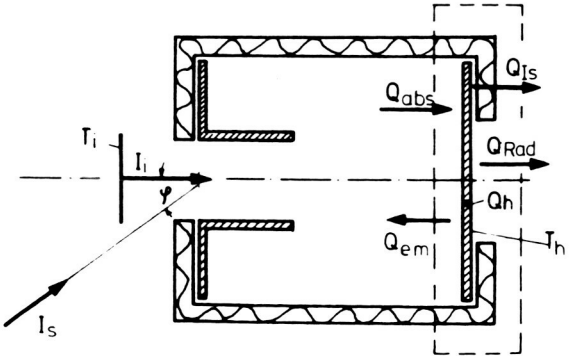

Fig. 5 Principle of aperture test body

As far as not yet defined earlier, the meaning of the designations shown in figure 5 is the following:

Q_{cm} : Heat emitted by heater plate

Q_{Is} : Heat loss of heater plate across superinsulation

Q_{Rad}: Heat emitted by radiator area of heater plate

I_i : Intensity of infrared heater

Generally a thermal balance holds:

$$Q_{abs} - Q_{em} - Q_{Is} - Q_{Rad} + Q_h = 0 \qquad (6)$$

For solar irradiation (I_s, φ) equation (6) by adding the parameters in brackets can be more fully written by

$$Q_{abs}(I_s, \varphi, T_h) - Q_{em}(T_h) - Q_{Is}(T_h) - Q_{Rad}(T_h) + Q_h(I_s, \varphi, T_h) = 0 \qquad (7)$$

For irradiation by an infrared heater correspondingly holds:

$$Q_{abs}(I_i, T_h) - Q_{em}(T_h) - Q_{Is}(T_h) - Q_{Rad}(T_h) + Q_h(I_i, T_h) = 0 \qquad (8)$$

Without irradiation ($I_s=0$, $I_i=0$ respectively)
eq. (7) and (8) reduce to

$$Q_{abs}(I=0, T_h) - Q_{em}(T_h) - Q_{Is}(T_h) - Q_{Rad}(T_h) + Q_h(I=0, T_h) = 0 \qquad (9)$$

If the heater plate in case without irradiation is heated to the same temperature T_h as in case with irradiation (I_s, φ, I_i respectively) from eq. (7), (8) and (9) can be derived that

$$Q_{abs}(I_s, \varphi, T_h) - Q_{abs}(I=0, T_h) = Q_h(I=0, T_h) - Q_h(I_s, \varphi, T_h) \qquad (10)$$

or

$$Q_{abs}(I_i, T_h) - Q_{abs}(I=0, T_h) = Q_h(I=0, T_h) - Q_h(I_i, T_h) \qquad (11)$$

respectively.

As the heat irradiated to sensor apertures is independent of heater plate temperature T_h, it can be concluded that the differences in absorbed heat and the differences of heater powers, respectively, are essentially independent of T_h. This was proven by tests and can be expressed by the following equations:

$$\Delta Q_h(I_s, \varphi) = Q_h(I=0,T_h) - Q_h(I_s, \varphi, T_h), \quad (12)$$

$$\Delta Q_h(I_i) = Q_h(I=0,T_h) - Q_h(I_i,T_h) \quad . \quad (13)$$

Furthermore, in tests the expected proportionality between heater power difference and intensity was proven, which can be expressed by

$$\Delta Q_h(I_s, \varphi) = C_{1s}(\varphi) . I_s \quad (14)$$

and

$$\Delta Q_h(I_i) = C_{1i} I_i \quad , \quad (15)$$

with $C_{1s}(\varphi)$ and C_{1i} being proportional constants.
In general the net heat input to a sensor aperture is

$$Q_{net} = Q_{abs} - Q_{em} \quad . \quad (16)$$

Using eq. (10), (11), (12) and (13) equation (14) can be written in the forms

$$Q_{net}(I_s, \varphi, T_h) = \Delta Q_h(I_s, \varphi) + Q_{net}(I=0,T_h) \quad (17)$$

and

$$Q_{net}(I_i, T_h) = \Delta Q_h(I_i) + Q_{net}(I=0,T_h) \quad (18)$$

respectively.

Corresponding to eq. (9) the net heat input in case without irradiation (I=0) can be determined by

$$Q_{net}(I=0,T_h) = Q_{Is}(T_h) + Q_{Rad}(T_h) - Q_h(I=0,T_h) \quad (19)$$

with

$$Q_{Is}(T_h) = \varepsilon_{Iseff} \cdot A_{Is} \cdot \sigma T_h^4 \quad (20)$$

and

$$Q_{Rad}(T_h) = \varepsilon_{Rad} \cdot A_{Rad} \cdot \sigma T_h^4 \quad , \quad (21)$$

where

ε_{Iseff}, ε_{Rad} are the quite accurately known effective emittances of the insulation and the heater plate radiator, respectively, and

A_{Is}, A_{Rad} are the areas of the insulation and the radiator, respectively.

$Q_{net}(I=0,T_h)$ is always negative. It is obvious that $Q_{net}(I=0,T_h)$ is only dependent on T_h. In fact, tests showed the expected result that $Q_{net}(I=0,T_h)$ is essentially proportional to T_h^4. The functional dependency

$$Q_{net}(I=0,T_h) = -C_2 \cdot T_h^4 \quad , \tag{22}$$

with C_2 being a proportional constant, can be easily determined by testing the aperture test body without irradiation.

With eq. (14), (15) and (22) the eq. (17) and (18) are rearranged to

$$Q_{net}(I_s, \varphi, T_h) = C_{1s}(\varphi) \cdot I_s - C_2 \cdot T_h^4 \tag{23}$$

and

$$Q_{net}(I_i, T_h) = C_{1i} \cdot I_i - C_2 T_h^4 \quad . \tag{24}$$

Based on the described theory the calibration of the infrared heater is done now in a quite simple manner:

The infrared heater, characterized by I_i or T_i^4, respectively, is irradiating exactly the same heat input as a simulated solar radiation, characterized by I_s and φ, into the sensor aperture, if for identical heater plate temperature the heater powers $Q_h(I_i,T_h)$ and $Q_h(I_s,\varphi,T_h)$ or $\Delta Q_h(I_i)$ and $\Delta Q_h(I_s,\varphi)$, respectively, are of equal magnitude.

By few measurements a correlation between solar irradiation (I_s,φ) and infrared radiation (T_i^4) can be established and, in principle, is shown in figure 6.

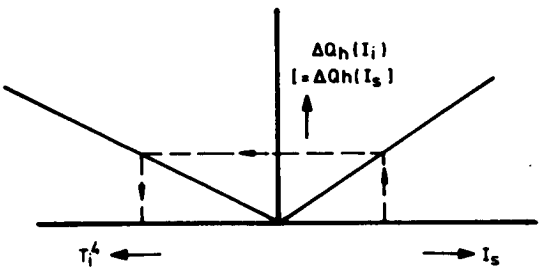

Fig. 6 Functional dependency between solar intensity I_s and infrared heater temperature T_i with infrared heater power difference $\Delta Q_h(I_i)$ as coupling parameter

The evaluated constants C_1 and C_2 can be used as input data for the mathematical model of the probe. If for a sensor aperture node C_1 is used at the place where usually $\alpha_s \cdot e_s \cdot A$ is introduced and C_2 is used at the place where usually $\varepsilon_h \cdot e_{h \to Space} \cdot A \cdot \sigma$ is introduced, the net heat input to the sensor aperture is taken into account correctly, inspite of $C_1 \cdot I_s$ not being identical to the absorbed heat Q_{abs} and $C_2 \cdot T_h^4$ not being identical to the emitted heat Q_{em}. In fact, from eq. (10) to (18) is derived that

$$C_1 \cdot I_s = Q_{abs}(I_s, \varphi, T_h) - Q_{abs}(I=0, T_h) \qquad (25)$$

and

$$C_2 \cdot T_h^4 = Q_{em}(T_h) - Q_{abs}(I=0, T_h) \quad . \qquad (26)$$

It is a specific advantage of the described method that the net heat input to sensor apertures can be determined in the same way without modifying the method, if the aperture funnels for sensor design reasons are covered by special foils or grids, etc.

Adaptation of the Aperture Heater Method to the Spinning Probe

Actually the HELIOS probe is spinning with an angular velocity of 60 r.p.m. and, therefore, the incident angle φ varies rapidly. Provided that the rotation of the probe is sufficiently rapid, such that the sensor temperature remains essentially time independent - which actually is the case for 60 r.p.m. angular velocity - the mean, during one revolution experienced heat input $\bar{Q}_{net}(I_s, T_h)$ corresponding to eq. (17) is

$$\bar{Q}_{net}(I_s, T_h) = \overline{\Delta Q}_h(I_s) + Q_{net}(I=0, T_h) \qquad (27)$$

with

$$\overline{\Delta Q}_h(I_s) = \frac{1}{2\pi} \int_0^{2\pi} Q_h(I_s, \varphi) \, d\varphi \quad . \qquad (28)$$

The experimental evaluation of the integral $\overline{\Delta Q}_h(I_s)$ usually requires a considerable testing effort as the aperture test body has to be mounted in a vacuum chamber on a spin table and the lines for temperature measurement and power supply have to be led across slip rings.

The effort, however, can be reduced if the integral is approximated by a sum. In this case ΔQ_h can be measured for some constant incident angles φ_{n_1} and φ_{n_2}, with

$$\varphi_{n_1} = n_1 \cdot \frac{\pi}{2N} \quad , \quad n_1 = 0, 1, 2, \ldots N \tag{29}$$

and

$$\varphi_{n_2} = n_2 \cdot \frac{\pi}{2N} \quad , \quad n_2 = -1, -2, \ldots -N \, , \tag{30}$$

and, based upon this, $\overline{\Delta Q_h}(I_s)$ can sufficiently accurately be determined by

$$\overline{\Delta Q_h}(I_s) = \frac{1}{N+1} \sum_{n_1=0}^{N} \Delta Q_h(I_s, \varphi_{n_1}) + \frac{1}{N} \sum_{n_2=-1}^{-N} \Delta Q_h(I_s, \varphi_{n_2}) . \tag{31}$$

In most cases tests for incident angles $\varphi_{n_1=N}$ and $\varphi_{n_2=-N}$ needed not to be performed, as for geometrical reasons

$$\Delta Q_h(I_s, \varphi_{n_1=N}) = \Delta Q_h(I_s, \varphi_{n_2=-N}) = 0$$

was obvious.

Moreover tests for all incident angles φ_{n_2} could be cancelled, if for symmetry reasons apparently

$$\Delta Q_h(I_s, \varphi_{n_1}) = \Delta Q_h(I_s, \varphi_{n_2=-n_1})$$

held.

Thus the number of these steady state temperature tests could be kept within reasonable limits.

SPECIFIC VALUE OF HELIOS INFRARED TEST TECHNIQUE

Somewhat paradoxically, the specific value of the HELIOS infrared test technique is based on the fact that in most cases Step 1 of the sequence has not to be carried out, because the absorptances of the surface are fairly accurately (tolerance: ± 0,02) known from measurements of small samples and, therefore, the absorbed radiation Q_{abs} can be determined due to eq. (1).

In fact for HELIOS the costly and in many cases - because of the lack of sufficiently powerful Xenon arc solar simulators for high intensities - impossible solar simulation tests of Step 1 could be avoided for all surfaces except for the sensor apertures.

For the cylindrical heat shield section covered by second surface mirrors and nearly ideally insulated from the probe central body even Step 1 and Step 2 needed not to be performed. In this case the temperature of the heat shields was only dependent on the solar absorptance and the emittance of the heat shield surface and, as these data very accurately could be determined by spectral measurements on small samples, the heat shield temperature could easily and accurately be calculated. The corresponding infrared heater section during Step 3 just had to be heated such that the calculated heat shield temperature was met.

A further essential advantage of the described infrared testing principle is the fact that all macroscopic temperature gradients along the spacecraft surfaces are generated without any additional effort just as they are generated under real solar irradiation. Although the heat generation within an infrared heater section is exactly uniformly distributed and, therefore, net heat flux from infrared heater to surface is uniform over the total surface area, the infrared heaters under discussion not necessarily will be isothermal. They, of course, do adjust their temperature distribution to gradients within the irradiated surfaces. This, by the way, is the reason why infrared heaters of the described kind should have an as low as possible thermal conductance in surface direction.

DESIGN ITEMS

The Thermal Canister consists of a thin aluminium sheet structure with heater foils glued to the outside of the sheets. The space-viewing side is coated with a high emissivity paint in order to enhance radiative heat exchange with the spacecraft (Fig. 7).

Following equation (2) the net heat transfer between canister and spacecraft and consequently the heat to be generated per unit area in the canister depends on the thermo-optical properties of the spacecraft section irradiated. In this respect HELIOS is divided into three main sections: the upper solar array, the center body, and the lower solar array. Thus the canister is divided into three corresponding sections which are thermally insulated from each other by fibreglass stand-offs and by mirror foils. In the centerbody section special heaters are incorporated for the experiment apertures in the heat shield.

The three sections and each of the aperture heaters can be separately electrically controlled. The installed power is 9,8 kW in each solar array section and 2 kW in the centerbody section. Because the thermal canister is to be used for the prototype and flight spacecraft the heaters are supplied with stabilized dc voltage (max. 200 V), and the heater mats are designed to generate a sufficiently low electro-magnetic

field in order not to disturb the spacecraft operation during testing.

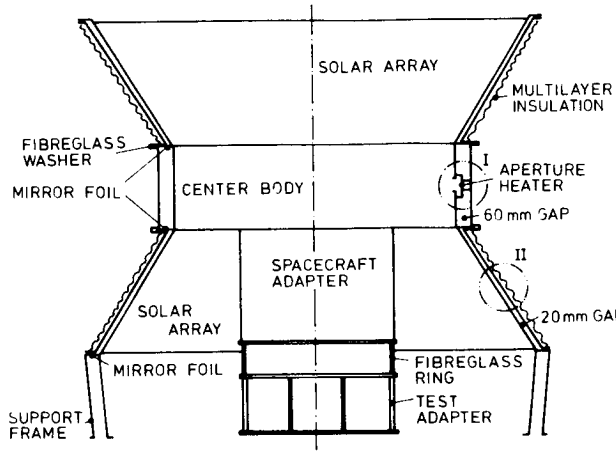

Fig. 7 Thermal Canister design

In order to reduce the heater power needed, the solar array sections are covered by multilayer insulation blankets on the outside. The centerbody section has a bare outside with an emissivity adjusted so that the coupling of the heat shield to the cold shroud of the test chamber is sufficient to cool the heat shield to the 1 AU conditions low temperatures (Fig. 8).

The canister is mounted on studs around the spacecraft without direct conductive contact to the spacecraft skin. For mounting purposes it is divided into two halfs in axial direction.

Special Design Problems

For the simulation of the net heat flux to the solar arrays at 16 S.C. the canister has to be heated to 230 °C. For the non-metallic materials and components involved this presented many problems which in most cases could only be solved by tests and special developments. MINCO Products Inc. produced a special type of thermofoil heater out of Kapton which has the required power per unit area and temperature resistivity. The heaters are glued to the structure by Bloomingdale FM 150-2u adhesive which has to be cured at 150 °C under vacuum pressure. Midland Industries Sicon 8 x 906 black paint was found to have the required emissivity, temperature stability and low outgassing characteristics.

For the experiment aperture heaters which reach 350 °C the problems were even more severe. The heaters used here are Philips Thermocoax wires which are hard-soldered into a stainless steel plate. The high emissivity surface is achieved by an anorganic paint (IIT's IITRI-Z 93), the mirror foils reducing heat exchange with the surrounding heat shield are Kapton foils aluminized on both sides (Fig. 9).

Fig. 8 HELIOS Thermal Canister

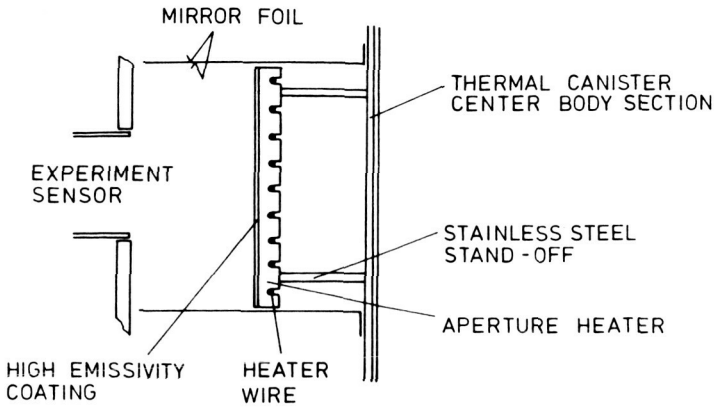

Fig. 9 Aperture heater design

COMPARISON OF THERMAL CANISTER AND SOLAR SIMULATION TESTS

Since the validity of the infrared test technique is of some importance to the success of the HELIOS mission, the thermal canister test results are verified in the thermal model test program by solar simulation tests at the highest possible intensities. The solar simulation tests have been performed at 0.9 S.C., 4.5 S.C. and 7.4 S.C. with the complete model in a Xenon arc light beam (Fig. 10).

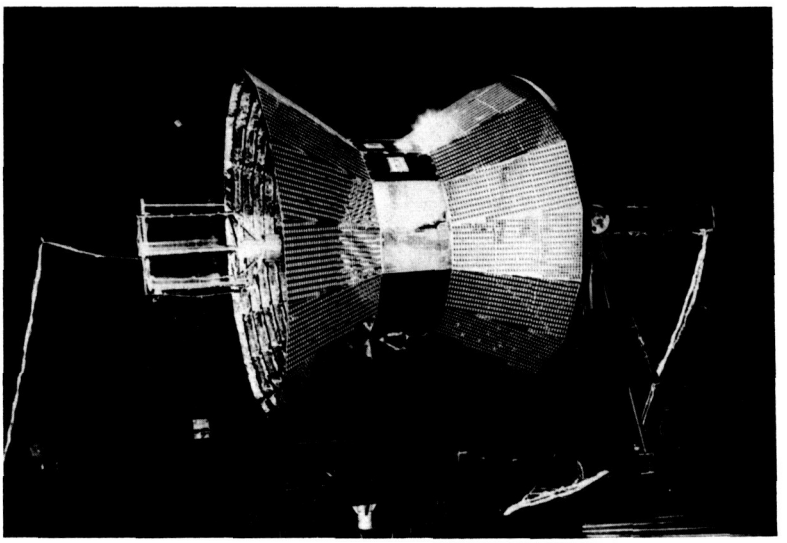

Fig. 10 HELIOS solar simulation test

In Fig. 11 the temperatures of the solar array and heat shield as measured in solar simulation tests and in canister tests are displayed. The temperatures of the solar arrays and the heat shield measured during both kinds of tests are in good agreement for the three solar intensities mentioned. For the 7.4 S.C. solar simulation test the temperature of the outer end of the lower solar array is considerably lower than the temperature of this part for the corresponding canister test, because at this intensity the solar light beam diameter was not big enough to cover this part of the spacecraft too.

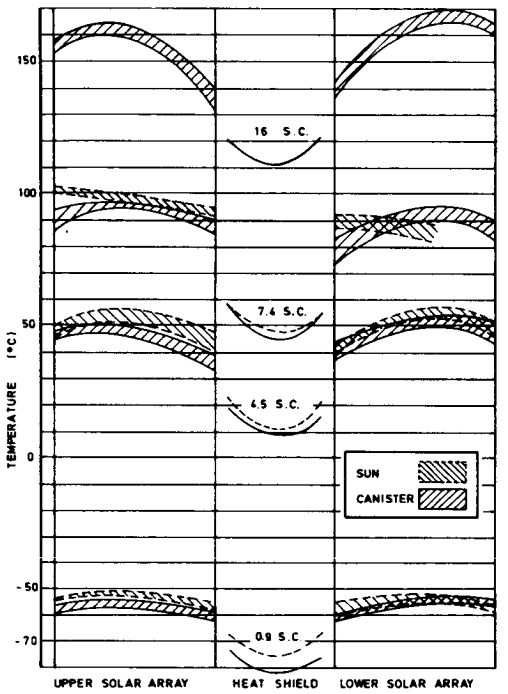

Fig. 11 HELIOS spacecraft skin test temperatures

Fig. 12 gives an analysis of the temperature difference between both kinds of tests at 0.9 S.C. and 7.4 S.C. for internal components based on measurements of about 170 sensors.

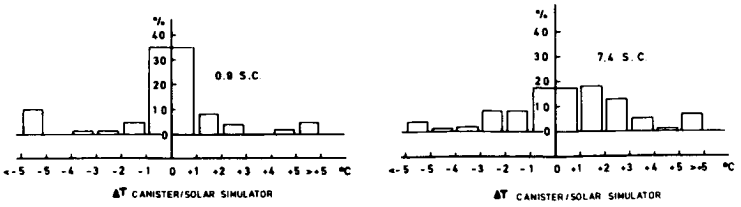

Fig. 12 Temperature difference between canister and solar simulation test of internal components at 0.9 S.C. and 7.4 S.C.

Apparently the agreement of internal component temperatures for both kinds of tests is good, too. The few differences of $\pm$ 5 °C or more are due to a change in dissipation in one compartment of the centerbody between canister and solar simulation test. A detailed evaluation of the solar simulation test also verifies the aperture heat input determination. The analytical model which takes the aperture test results into account duplicates the solar simulation test temperatures for the experiments with apertures.

CONCLUSION

The tests performed indicate that the infrared test technique developed for the HELIOS spacecraft gives identical results as solar simulation tests at low and medium intensities. Therefore, the extrapolation to the highest intensity of the mission seems to be valid.

It is the conviction of the authors that the described infrared heater technique can be advantageously applied in practically all cases, in which either the required simulated solar intensity or the required magnitude of illuminated area (or both) cannot be fulfilled by existing or available Xenon arc lamp solar simulation sources.